Chapter 9
Performance Evaluation of Segmentation Algorithms in Non Contrast and Contrast MRI Images for Region of Interest

S. Prabhu Das, B. N. Jagadesh, and B. Prabhakara Rao

Introduction

Biomedical Image Processing is the now becoming an emerging field in health monitoring, diagnosis and to treat different kinds of internal organ abnormalities or diseases for scientific study or treatment [1].

Medical Imaging [2] is an in vivo imaging process and it involves visualisation of internal organs within the body of humans or animals using non-invasive imaging modalities such as X-Ray, CT, MRI, PET Scans, etc. with the help of computer aids. Computer Aided Diagnosis (CAD) helps the medical expert to acquire better anatomical structures and to study the Region of Interest (ROI) within the tissue.

CAD tools involve the expert to automate the process [3], to get the results fast and accurately even for large number of cases without fatigue or data overload at minimal cost. They support remote accessing using information technologies through faster communication in case of emergency.

Imaging Modalities and Their Contrast Media

There are many imaging modalities [4] are used in biomedical engineering. They are Computed Tomography (CT), Magnetic Resonance Imaging (MRI), Ultrasound (US) Imaging, Digital Mammography, Positron Emission Tomography (PET) and

S. Prabhu Das (✉) · B. Prabhakara Rao
Department of Electronics and Communication Engineering, JNTUK, Kakinada, India
e-mail: spdas3607@gmail.com

B. N. Jagadesh
School of Computer Science and Engineering, VIT-AP University, Amaravathi, India

Thermal Imaging and so on. Each and every modality has its own strengths and weaknesses but they are application specific. For example, X-Ray Imaging is mainly used to visualise hard tissues such as bones within the body whereas CT and MRI imaging modalities are used to observe soft tissues or both. These processes include Ionisation and electromagnetic interferences at microscopic level, respectively.

CT: Computed Tomography (CT) as the name indicates that the computer creates the images sequence by taking the inputs from X-Rays at all possible angles around the object in the form of slices called Tomograms. CTs produce the pictorial information of the object using ionising radiation. It can visualise brightly the high-density matters such as bones, calcium and high densities and darkly the low-density matters such as liquids fats, etc. The Hounsfield units are used to represent the different densities measured. For example, Water typically having 0 HU may be varying between -7 to $+7$ HU, bones have higher densities greater than 500 HU, soft tissues within the range 10–60 HU and fats with low density between -25 HU to -250 [5].

Modern CT scanners are advantageous that they can scan the abdomen and pelvis very quickly at a slice thickness of less than 1 mm within the span of 6–7 s per view. This is better suitable for the case of children without giving anaesthesia. Detailed information about any tissue is also obtained by other projections such as Sagittal and Coronal. CT scanners can also produce 3D scans [5].

CT scanners produce high-resolution images with minimal noise but are unable to detect inflammation defects.

MRI: MRI [6] is a non-ionising modality in radio imaging and it is extensively used for imaging soft tissues, organs, bone and other internal structures because it offers much greater contrast between the diverse soft tissues of the body. It is mostly used in radiology to diagnose or monitor treatment for abnormal conditions or staging the disease within the chest, abdomen and pelvis. MRIs produce very good contrast images of soft tissues compared to CTs. The human body naturally consists of hydrogen atoms within the body. MRI consists of a powerful rotating magnet, electric field gradients [7] (induction coils) and a digital computer to form images. The protons within the hydrogen atoms of water molecules are having magnetic properties such that all protons are aligned parallel to the main magnetic field. In MRI, a strong magnetic field is applied to line up the nuclear magnetisation of hydrogen atoms of the observing part of the body. An RF signal from the induction coils is applied subsequently in the form of RF pulses to alter the alignment of the protons and reversed to get relaxation energy from the protons. This relaxation energy is detected by MRI scanners to construct the image using K-space [8]. By changing the parameters of this RF pulse sequence, different contrasts may be generated between tissues based on the relaxation properties of the hydrogen atoms there in the tissues.

Depending on relaxation times and dynamic contrast variations [9], the intensities within the image are correlating with the tissue characteristics. It can produce morphological and functional information about the tissue without any ionising radiation.

PET: Positron Emission Tomography (PET) [10] is a functional imaging technique used to obtain the information about the changes in metabolic process, oxygen

through the blood flow and tissues or organs' working conditions. It is the combination of nuclear medicine and biochemical interactions with the body of observation. PET scans are mostly used for monitoring the functioning of brain disorders, heart problems and cancer cells within the body. PETs employ radioactive tracers that were swallowed as gas or injected into the body parts being examined. These tracers chemically react differently with the different parts of the body. These differential changes will be collected by the PET scanners as bright spots if they were infected. PET scanners can able to measure the oxygen [11] and sugar levels of the body and early stages of defects which are not possible by other scanners at cellular level. In PETs, gamma cameras are used to produce and to collect gamma rays as similar to X-rays. High chemical reaction of tracers will be shown as hot spots with greater intensity and less chemical reactions as cold spots with light intensities. Cancer cells [12] have high metabolic rate viewed as hot spots than non-cancer cells. Healthy tissues have more tracer absorption than the diseased one. Thus the level of heart problems was detected based the degree of interaction and colour differentiation. PET scanners are also used for detecting problems through the interaction of tracer with the glucose such as Alzheimer's disease [13], depression, epilepsy, head and Parkinson's disease in central nervous system. PETs also used with CT/MRI to get more information about disease.

PET scans are less accurate in case of small-sized tumours and at high blood sugar levels.

Microscopy [14] and PA imaging techniques [15] with contrasts are useful to detect defects from the defected organs due to deeper penetration.

According to our findings [16], ultrasonography examination could be used as a preliminary assessment for stratifying patients based on their risk of ADPKD progression. Because of the low accuracy and reproducibility of ultrasound, this estimate should only be used for patients with kidney volumes that are close to normal. A first magnetic resonance imaging (MRI) scan is recommended for dimensional increases in kidney size.

Contrast Materials: To improve medical imaging, various types of contrast media have been utilised. These contrast materials can be injected into veins or arteries, spinal discs or fluid spaces and other bodily cavities. Contrast materials come in a variety of forms:

1. X-ray and computed tomography (CT) imaging exams use iodine-based and barium-sulfate chemicals. The most often used contrast substance is barium-sulfate, which is administered orally. It is also administered rectally and comes in a variety of forms. Iodine-based and barium-sulfate contrast materials block or limit the ability of X-rays to pass through a specific area of the body. As a result, blood vessels, organs and other bodily tissue containing iodine-based or barium compounds on X-Ray or CT pictures change appearance.

2. Gadolinium is a key component of the most used magnetic resonance (MR) contrast material. When this chemical is present in the body, it changes the magnetic properties of adjacent water molecules, improving the quality of magnetic resonance imaging (MRI) images. Thus, internal soft organs, such

(a) MRI Image without Contrast   (b)MRI Image without Contrast
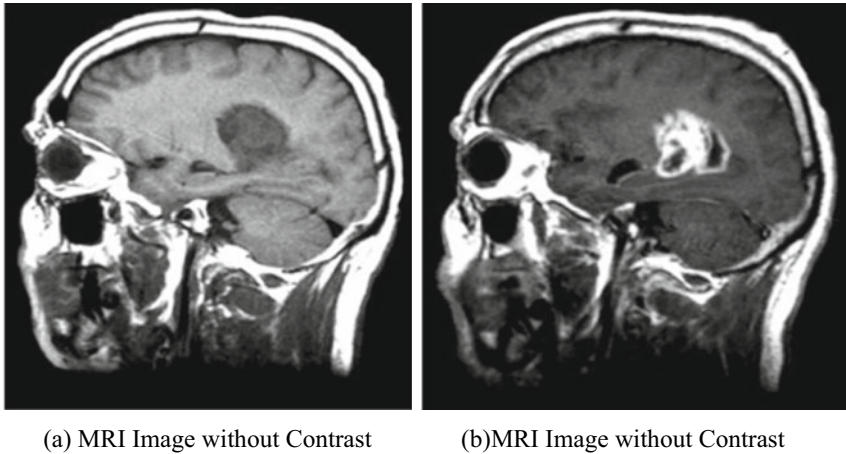
Fig. 9.1 Illustration example for non-contrast and Gd Contrast MRI images. *Source* https://home.physics.wisc.edu/gilbert/wp-content/uploads/sites/3/2017/08/mri.gif

as the heart, lungs, liver, adrenal glands, kidneys, pancreas, gall bladder, spleen, uterus and bladder are monitored.

3. In imaging studies, saline (salt water) and gas (such as air) are also employed as contrast materials. Ultrasound imaging exams, particularly those of the heart, have used microbubbles and microspheres. Blood perfusion in organs is assessed using contrast-enhanced ultrasonography with microbubbles [17], thrombosis, such as in myocardial infarction, cardiac anomalies, liver and kidney tumours, inflammatory activity in inflammatory bowel illness and reaction to chemotherapy treatment (Fig. 9.1).

Proposed Methodology

In this paper, the proposed block diagram as shown in Fig. 9.2 is a new combination of denoising algorithms used to improve the image quality and to enhance the image contrast before segmenting the MRI Image. The image quality is improved by reducing the noise present within the image using Adaptive NLM Algorithm and contrast is enhanced using CLAHE algorithm. The Region of Interest (ROI) to be segmented in contrast-enhanced image is compared with the same in contrast image obtained from the subject injecting the contrast agent. The segmentation performance is compared in terms of its characteristics such as Sensitivity or Recall, Specificity, DICE and Jaccardian Coefficients.
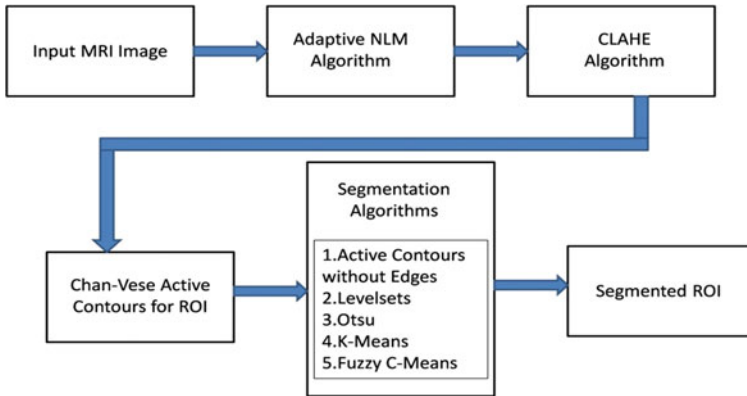
Fig. 9.2 Block diagram of the proposed methodology

Preprocessing of MRI Images

There are several image denoising techniques available, then Non-local filters are widely used in the area of MR imaging [18, 19].

Advantages of NLM Algorithms

- The NLM noise reduction algorithm, in particular, was devised to minimise the loss of underlying image information while selectively removing only the noise.
- After setting areas with the same sized mask positioned around the region of interest, this technique assesses the similarity of the intensity and edge information in a picture (ROI).
- Furthermore, the higher the allocated weight employed during picture processing, the higher the degree of similarity.

In terms of PSNR, MSE and SSIM, experimental results shown in [20] on standard images indicate that the adaptive NLM algorithm outperforms the traditional NLM algorithm.

Contrast Limited Adaptive Histogram Equalisation (CLAHE)

A CLAHE algorithm [21] limit the amplification by clipping the histogram. It has two key parameters: Block Size (BS) and Clip Limit (CL). These two parameters improve the brightness and contrast of the image, respectively.

The CLAHE method to enhance the original image consists of the following steps:

Step 1: initially the input Image is dividing into non-overlapping contextual regions equal to $M \times N$.

Step 2: Histogram is calculated for each contextual region.

Step 3: Calculate the Clip Limit (CL) for each region as given below

$$N_{\text{avg}} = \frac{N_r(x)N_r(y)}{N_{\text{gray}}} \tag{9.1}$$

where N_{avg} is the average number of pixels, N_{gray} is the number of gray levels in the contextual region, $N_r(x)$ and $N_r(y)$ are the numbers of pixels in the X dimension and Y dimension of the contextual region. Then the actual CL is

$$N_{\text{CL}} = N_{\text{clip}} N_{\text{avg}} \tag{9.2}$$

where N_{clip} is the normalised CL in the range of [0, 1]. If the number of pixels is greater than N_{CL}, the pixels will be clipped. The total number of clipped pixels is defined as $N_{\sum \text{clip}}$ then the average of the remain pixels to distribute to each gray level is

$$N_{\text{avggray}} = \frac{N_{\sum \text{clip}}}{N_{\text{gray}}} \tag{9.3}$$

The histogram clipping rule is given by the following statements

$$\text{If } H_{\text{region}}(i) > N_{\text{CL}} \text{ then } H_{\text{region\_clip}}(i) = N_{\text{CL}} \tag{9.4}$$

$$\text{Else if } H_{\text{region}}(i) + N_{\text{avggray}} > N_{\text{CL}} \text{ then } H_{\text{region\_clip}}(i) = N_{\text{CL}} \tag{9.5}$$

$$\text{Else } H_{\text{region\_clip}}(i) = H_{\text{region}}(i) + N_{\text{CL}} \tag{9.6}$$

where $H_{\text{region}}(i)$ and $H_{\text{region\_clip}}(i)$ are original histogram and clipped histogram of each region at i-th gray level.

Step 4: Redistribute the remaining pixels until the remaining pixels have been all distributed. The step of redistribution of pixels is given by

$$\text{Step} = \frac{N_{\text{gray}}}{N_{\text{remaining}}} \tag{9.7}$$

where $N_{\text{remaining}}$ is the remaining number of clipped pixels. *Step* is positive integer at least 1.

Step 5: Then intensity values are distributed according to Rayleigh distribution to enhance the contrast and re-scaled using linear contrast stretching.

Step 6: To eliminate artefacts in the image, new gray level is calculated and assigned to the pixels in contextual region using bilinear interpolation.

Selection and Segmentation of ROI

The Region of Interest to be segmented within the MRI Image is selected manually and Chan-Vese Active Contours [22] was applied to get the object of the image. Manually the Mask will be drawn surrounding the ROI of the object for both CLAHE-enhanced and Contrast-enhanced images. Then efficiency of algorithm is estimated in terms of image characteristics.

Popular Segmentation Algorithms

Here we have taken the threshold-based and clustering algorithms which are useful for Medical Image segmentation applications. They are simple and popular algorithms, such as Otsu Algorithm [23], Active Contours without edges, Level sets [24], K-Means Segmentation [25] and Fuzzy C-Means Segmentation Algorithm [26]. They all are familiar and very simple to understand. Each algorithm has its own advantages and they are application specific.

Performance Metrics

This paper taken spatial overlap-based metrics [27] into account to evaluate the segmentation performance of each algorithm. These are derived from the cardinalities of confusion matrix such as namely the true positives (TP), the false positives (FP), the true negatives (TN) and the false negatives (FN). Then the derives metrics from these cardinalities are mostly used for segmentation evaluation are given by

$$\text{Recall} = \text{Sensitivity} = \frac{\text{TP}}{\text{FN} + \text{TP}} \tag{9.8}$$

This is also called True Positive Rate (TPR). Similarly, the True Negative Rate (TNR) is given by

$$\text{Specificity} = \text{TNR} = \frac{\text{TN}}{\text{FP} + \text{TN}} \tag{9.9}$$

Then

$$\text{DICE Coefficient} = \frac{2 * \text{TP}}{2 * \text{TP} + \text{FP} + \text{FN}} \tag{9.10}$$

This is called Overlap Index mostly used for validating Medical volume Segmentations. For the generalised segmentation with multiple labels, Jaccardian Index is considered.

$$\text{Jaccard Index} = \frac{\text{DICE Coefficient}}{2 - \text{DICE Coefficient}} \tag{9.11}$$

In this analysis, we have considered the above-mentioned four parameters to concise evaluation of segmentation.

Results and Discussions

The datasets were collected from publicly available TCIA database [28] browsing on the preferences as Imaging Modality: MR, Anatomical site: Kidney and Brain and Species: Homo sapiens excluding Phantoms. Totally there are 1043 subjects that were browsed. There are 82 categories of collections of kidney volumes in different projections and 961 categories of collections of Brain structures were obtained from different MRI machines such as GE MEDICAL SYSTEMS, SIEMENS, TOSHIBA_MEC and Philips Medical Systems with different subject IDs. We are mainly concentrate on Axial and coronal projections and selected 32 volumes with sizes 512×512 and 256×256, thicknesses of 4 mm, 5 mm,6 mm,7 mm, 8 mm and corresponding the spacing of 1.5 mm,2 mm,2.5 mm,3 mm,6 mm and 8 mm, respectively with and without Contrast media. From image volume sequence the slice with maximum tissue area was obtained from different series and then converted those into jpeg format. Each image used in this paper is mentioned with its ID, sequence number and slice number. The sequence/series number differentiates the projection series.
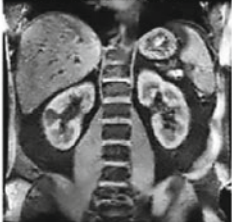
The kidney image shown in Fig. 9.3a is extracted for male subjects at an age of 41 years using GE MEDICAL SYSTEMS, COR KIDNEY1 PRE sequence with slice number 11 out of 20. It was obtained at a magnetic field strength of 1.5 T and Coronal 90 degrees flip angle projection with repetition time 160 s and echo time 1.344 s. The slice is with 256×256 size and the thickness of each slice is 5 mm with spacing 6 mm between them. This image is a non-contrasted image shown in Fig. 9.3i, it is preprocessed through Adaptive denoising algorithm to remove unwanted noise shown in Fig. 9.3ii, then contrast is enhanced and gray levels are distributed uniformly using CLAHE algorithm shown in Fig. 9.3iii. A Chan-Vese Active contour Algorithm is used to select the ROI manually and the proposed algorithms are employed for segmentation for both contrast and non contrast images.
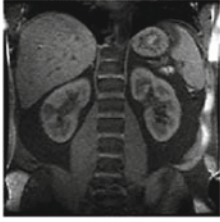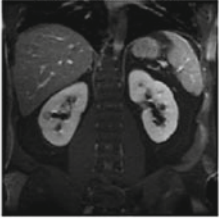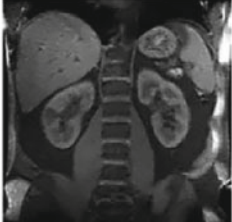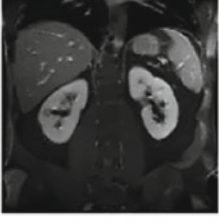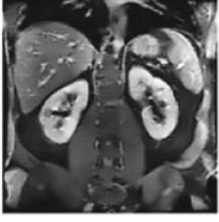
Similarly, the kidney image shown in Fig. 9.4a is extracted for male subjects at an age of 45 years using SEIMENS MEDICAL SYSTEMS, COR KIDNEY1 PRE sequence with slice number 30 out of 34.

It was obtained at a magnetic field strength of 1.5 T and Axial 90° flip angle projection with repetition time 120 s and echo time 1.156 s. The slice is with 256×256 sizes and the thickness of each slice is 5 mm with spacing 6 mm between them.

Conclusions

The proposed methodology is a new combination of Adaptive NLM Algorithm to reduce the noise in MRI images and CLAHE Algorithm is used to enhance the image contrast before segmenting the MRI Image. The Region of Interest (ROI) to be segmented in contrast-enhanced image is compared with the same in contrast image obtained from the subject injecting the contrast agent. The segmentation performance is compared in terms of its characteristics such as Sensitivity or Recall, Specificity, DICE and Jaccardian Coefficients as shown in Table 9.1 and their graphical evaluation is shown in Figs. 9.5 and 9.6.

The execution time in Fig. 9.6a shows that Otsu, K-Means and Fuzzy C-Means Algorithms are faster for both Non Contrast and Contrast MRI Images compared to the remaining algorithms. The sensitivity is less for Fuzzy C-Means due to soft computing and it is high for Otsu algorithms as shown in Fig. 9.6b. The specificity is more for contrast images in case of Fuzzy C-Means and it is less for Non Contrast image in case of Level set Segmentation. Finally, the DICE Coefficient and Jaccardian Indexes are similar for both Non Contrast and Contrast MRI Images and they are high for segmentation using Otsu Algorithm.

i. Input Image	Original Input Image (a) Non Contrast Image	Original Input Image (b) Contrast Image
ii.Denosing Image Using Adaptive NLM Algorithm	Adaptive NLM Filtered Image (a) Non Contrast Image	Adaptive NLM Filtered Image (a) Non Contrast Image
iii.Output of CLAHE Algorithm	CLAHE Processed Image (a) Non Contrast Image	CLAHE Processed Image (a) Non Contrast Image
iv.Mask used for Region Of Interest(ROI)	Initial MASK (a) Non Contrast Image	Initial MASK (a) Non Contrast Image

Fig. 9.3 Segmentation process for both non contrast and contrast MRI images-coronal direction
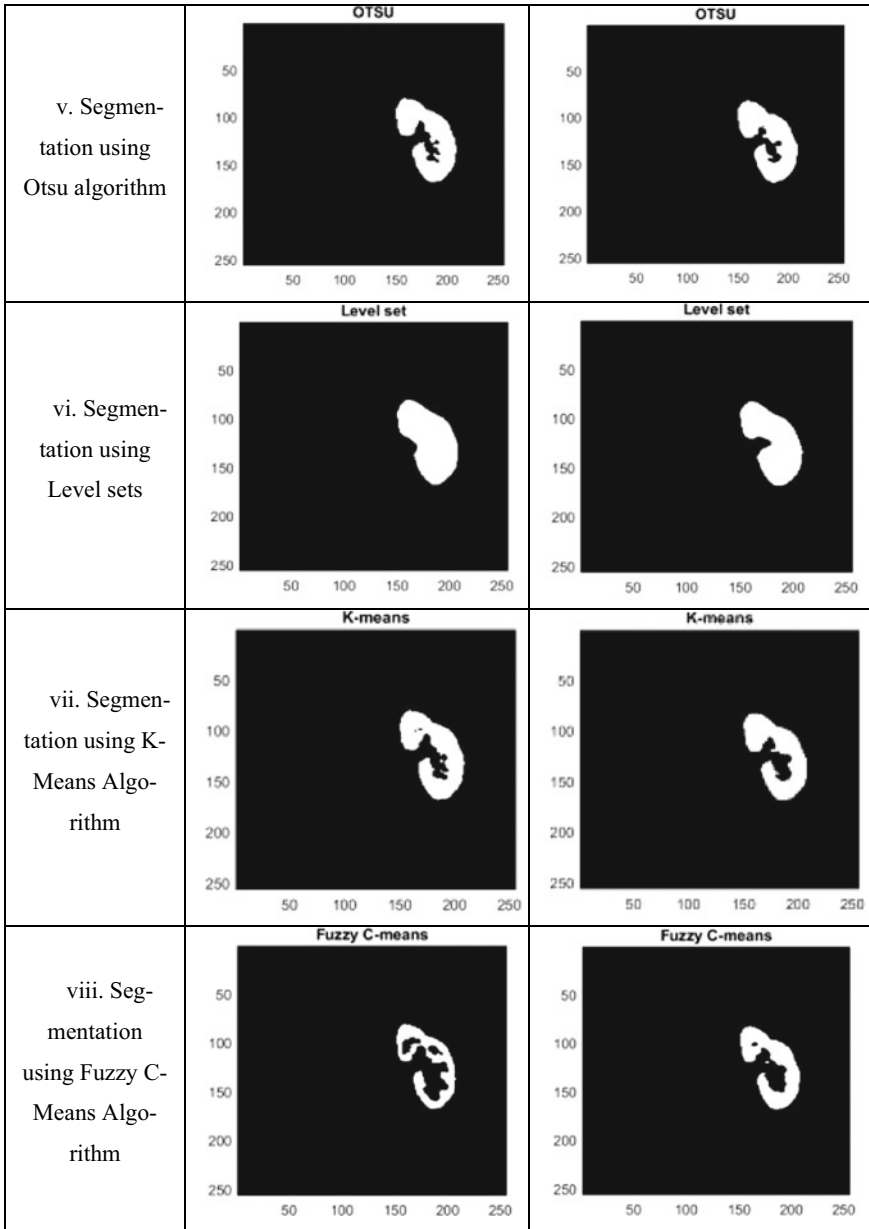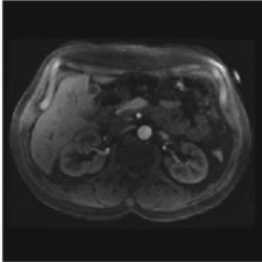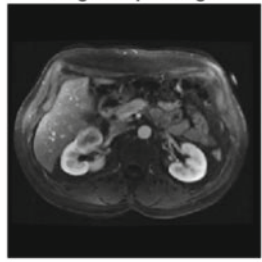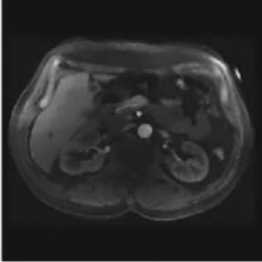
v. Segmentation using Otsu algorithm	OTSU	OTSU
vi. Segmentation using Level sets	Level set	Level set
vii. Segmentation using K-Means Algorithm	K-means	K-means
viii. Segmentation using Fuzzy C-Means Algorithm	Fuzzy C-means	Fuzzy C-means
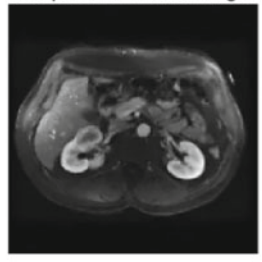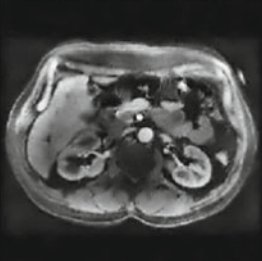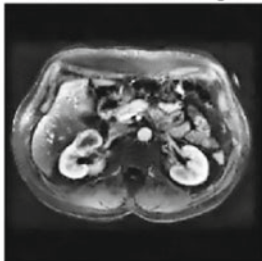
Fig. 9.3 (continued)

i. Input Image	Original Input Image	Original Input Image
ii. Denoising Image Using Adaptive NLM Algorithm	Adaptive NLM Filtered Image	Adaptive NLM Filtered Image
iii. Output of CLAHE Algo-rithm	CLAHE Processed Image	CLAHE Processed Image
iv. Mask used for Region Of Interest(ROI)	Initial MASK	Initial MASK

Fig. 9.4 Segmentation process for both non contrast and contrast MRI images-axial mode

v. Segmentation using Active Contours without Edges	AC without edges	AC without edges
vi. Segmentation using Otsu algorithm	OTSU	OTSU
vii. Segmentation using Level sets	Level set	Level set
viii. Segmentation using K-Means Algorithm	K-means	K-means
ix. Segmentation using Fuzzy C-Means Algorithm	Fuzzy C-means	Fuzzy C-means

Fig. 9.4   (continued)

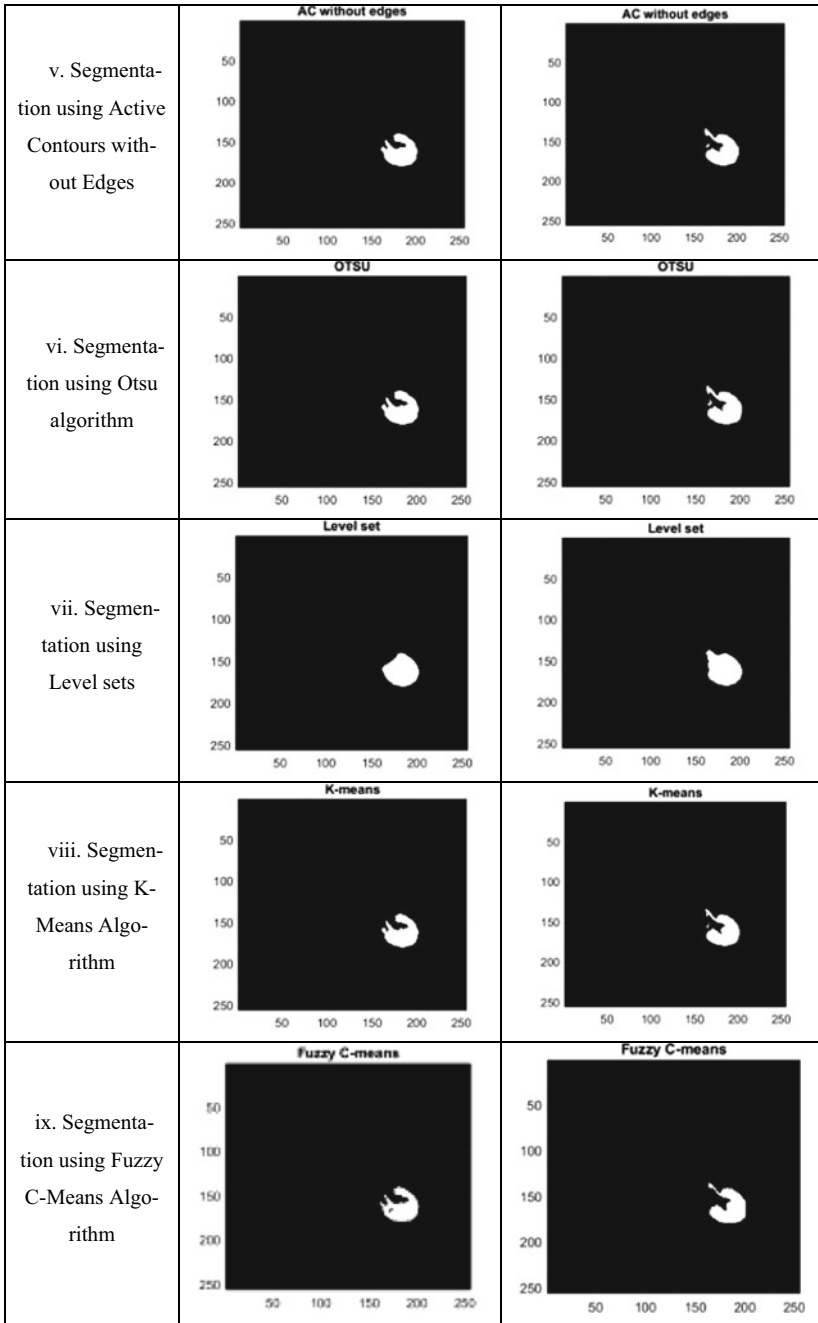**Table 9.1** Performance metrics comparison of non contrast and contrast MRI images (for Figs. 9.3 and 9.4)

Input MRI Image	Perf. metric	AC w/o Edges	Level sets	Otsu	K-Means	Fuzzy C-Means
Kidney 4807–11-11-WOC.jpg (Coronal Direction - without Contrast)	Time(in sec)	12.039859	24.186131	0.230866	0.25253	1.960667
	Sensitivity	0.9831	0.9482	0.9841	0.925	0.661
	Specificity	0.9975	0.992	0.9987	1	1
	DICE	0.9635	0.8904	0.9776	0.9605	0.7959
	Jaccard Index	0.9296	0.8024	0.9562	0.924	0.661
Kidney 4807-14-11-WC.jpg (Coronal Direction - with Contrast)	Time(in sec)	9.937055	22.565294	0.047243	0.286961	1.417538
	Sensitivity	0.9828	0.9386	0.9863	0.9016	0.8047
	Specificity	0.9991	0.9946	0.9993	1	1
	DICE	0.9815	0.9114	0.9859	0.9483	0.8918
	Jaccard Index	0.9637	0.8372	0.9722	0.9016	0.8047
Kidney 4989-13-45-WOC.jpg (Axial Direction - without Contrast)	Time(in sec)	9.411271	21.725564	0.02935	0.176253	1.816574
	Sensitivity	0.9885	0.9387	0.9933	0.9788	0.8949
	Specificity	0.9992	0.9976	0.9992	0.9997	1
	DICE	0.969	0.8987	0.9739	0.9807	0.944
	Jaccard Index	0.9399	0.816	0.9491	0.9621	0.894
Kidney 4989-14-45-WC.jpg (Axial Direction - with Contrast)	Time(in sec)	9.554764	21.924253	0.045166	0.199537	1.476591
	Sensitivity	0.976	0.9388	0.984	0.9547	0.8715
	Specificity	0.9996	0.9967	0.9997	1	1
	DICE	0.9769	0.8828	0.9832	0.9755	0.9313
	Jaccard Index	0.9549	0.7901	0.9669	0.9522	0.8715
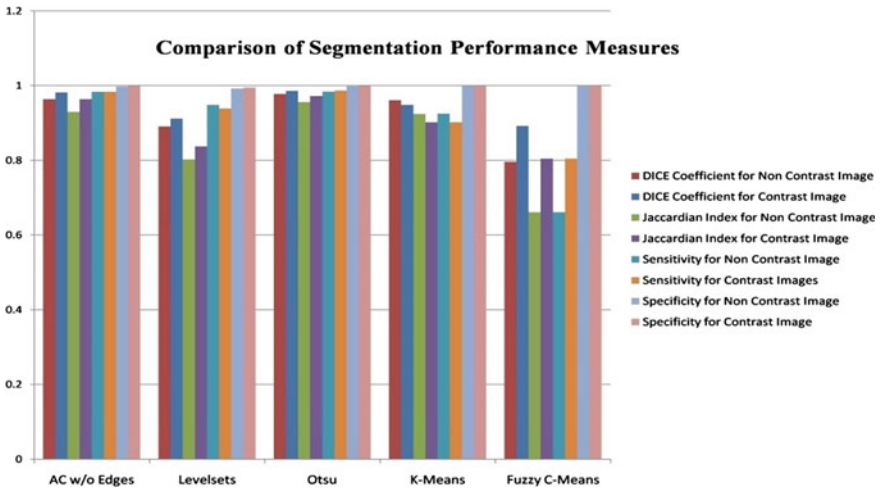
Fig. 9.5 Graphical representation of segmentation performance metrics

(a) Execution Time in Seconds

(b) Sensitivity

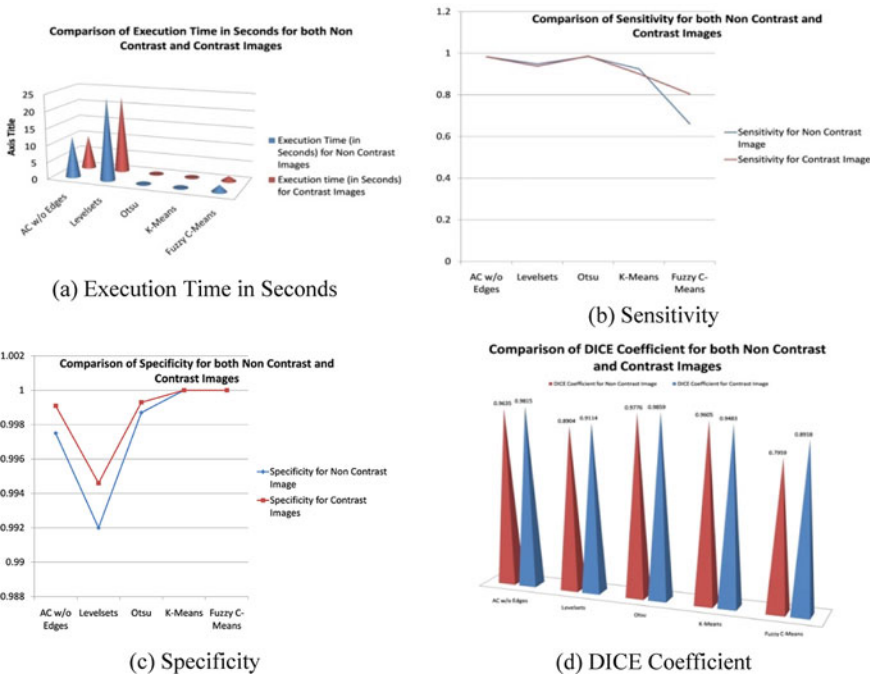(c) Specificity

(d) DICE Coefficient

Fig. 9.6 Graphical representation of individual segmentation performance metrics for non contrast and contrast images

References

1. Abdallah, Y.: Improvement of sonographic appearance using HATTOP methods. Int. J. Sci. Res. (IJSR) **4**(2), 2425–2430 (2015). https://doi.org/10.14738/jbemi.55.5283
2. Abdallah, O.M.Y., Alqahtani, T.: Research in Medical Imaging Using Image Processing Techniques, Medical Imaging—Principles and Applications, Yongxia Zhou, Intech Open (2019). https://doi.org/10.5772/intechopen.84360
3. Sharma, N., Aggarwal, L.M.: Automated medical image segmentation techniques. J. Med. Phys. **35**(1), 3–14 (2010). https://doi.org/10.4103/0971-6203.58777
4. Morris, P.: Biomedical Imaging, Woodhead Publishing, pp. xix–xxi (2014). ISBN 9780857091277
5. Hiorns, M.P.: Imaging of the urinary tract: the role of CT and MRI. Pediatr. Nephrol. **26**(1), 59–68 (2011). https://doi.org/10.1007/s00467-010-1645-4
6. Grattan-Smith, J.D., Jones, R.A.: MR urography in children. Pediatr. Radiol. **36**, 1229–1232 (2006). https://doi.org/10.1007/s00247-006-0222-2
7. Weishaupt, D., Koechli, V.D., Marincek, B.: How Does MRI Work?: An Introduction to the Physics and Function of Magnetic Resonance Imaging. Springer Science & Business Media (2013). ISBN 978-3-662-07805-1
8. Ljunggren, S.: A simple graphical representation of fourier-based imaging methods. J. Magn. Reson. **54**(2), 338–343 (1983)
9. Yankeelov, T.E., Gore, J.C.: Dynamic contrast enhanced magnetic resonance imaging in oncology: theory, data acquisition, analysis, and examples. Curr. Med. Imaging Rev. **3**(2), 91–107 (2009). https://doi.org/10.2174/157340507780619179
10. Bailey, D.L., Townsend, D.W., Valk, P.E., Maisy, M.N.: Positron Emission Tomography: Basic Sciences. Springer, Secaucus, NJ. 978-1-85233-798-8 (2005)
11. Azad, G.K., Siddique, M., Taylor, B., Green, A., O'Doherty, J., Gariani, J., et al.: 18F-Fluoride PET/CT SUV? J. Nucl. Med. **60**(3), 322–327 (2019)
12. Galway, K., Black, A., Cantwell, M., Cardwell, C.R., Mills, M., Donnelly, M.: Psychosocial interventions to improve quality of life and emotional wellbeing for recently diagnosed cancer patients. Cochrane Database Syst. Rev. **11**, CD007064 (2012). https://doi.org/10.1002/14651858.cd007064
13. Dementia: Quick Reference Guide (PDF). (UK) National Institute for Health and Clinical Excellence, London. November 2006. ISBN 978-1-84629-312-2
14. Thomas, G., et al.: Measuring the mechanical properties of living cells using atomic force microscopy. J. Visualized Experiments: JoVE **76**, 50497 (2013). https://doi.org/10.3791/50497
15. Jimmy, L.S., Karpiouk, A.B.,, Wang, B., Emelianov, S.Y.: Photoacoustic imaging of clinical metal needles in tissue. J. Biomed. Opt. **15**(2), 021309 (2010). https://doi.org/10.1117/1.3368686
16. Raghavendra, P., Pullaiah, T.: Advances in Cell and Molecular Diagnostics. Academic Press, pp. 85–111 (2018). ISBN 9780128136799. https://doi.org/10.1016/B978-0-12-813679-9.00004-X
17. Meloni, M.F., Smolock, A., Cantisani, V., et al.: Contrast enhanced ultrasound in the evaluation and percutaneous treatment of hepatic and renal tumors. Eur. J. Radiol. **84**(9), 1666–1674 (2015)
18. Bhujle, H.V., Vadavadagi, B.H.: NLM based magnetic resonance image denoising—a review. Biomed. Sign. Process. Control **47**, 252–261 (2019)
19. Buades, A., Coll, B., Morel, J.-M.: A non-local algorithm for image denoising. IEEE Comp. Soc. Conf. Comp. Vis. Pattrn. Recog. **2**, 60–65 (2005)
20. Verma, R., Pandey, R.: Non local means algorithm with adaptive isotropic search window size for image denoising. Ann. IEEE India Conf. (INDICON) **2015**, 1–5 (2015). https://doi.org/10.1109/INDICON.2015.7443193
21. Ma, J., Fan, X., Yang, S.X., Zhang, X., Zhu, X.: Contrast limited adaptive histogram equalization-based fusion in YIQ and HSI color spaces for underwater image enhancement. Int. J. Pattern Recognit. Artif. Intell. **32**, 1–26 (2018)

22. Chan, T.F., Vese, L.A.: Active contours without edges. IEEE Trans. Image Process. **10**(1), 266–277 (2001). https://doi.org/10.1109/83.902291
23. Wang, H., Dong, Y.: An improved image segmentation algorithm based on Otsu method. In: International Symposium on Photoelectronic Detection and Imaging 2007: Related Technologies and Applications, vol. 6625 (2008)
24. Li, C., Huang, R., Ding, Z., Gatenby, J.C., Metaxas, D.N., Gore, J.C.: A level set method for image segmentation in the presence of intensity inhomogeneities with application to MRI. IEEE Trans. Image Process. **20**(7), 2007–2016 (2011). https://doi.org/10.1109/TIP.2011.214 6190
25. Venkatachalam, K., Reddy, V.P., Amudhan, M., Raguraman, A., Mohan, E.: An implementation of K-means clustering for efficient image segmentation. In: 2021 10th IEEE international conference on Communication Systems and Network Technologies (CSNT), pp. 224–229 (2021). https://doi.org/10.1109/CSNT51715.2021.9509680
26. Rahman, T., Islam, M.S.: Image segmentation based on fuzzy C means clustering algorithm and morphological reconstruction. In: 2021 International Conference on Information and Communication Technology for Sustainable Development (ICICT4SD), pp. 259–263 (2021). https://doi.org/10.1109/ICICT4SD50815.2021.9396873
27. Taha, A.A., Hanbury, A.: Metrics for evaluating 3D medical image segmentation: analysis, selection, and tool. BMC Med. Imaging **15**, 29 (2015). https://doi.org/10.1186/s12880-015-0068-x
28. TCIA Database. https://nbia.cancerimagingarchive.net/nbia-search/